Inter-joint coordination to minimize angular momentum reduction in backward somersault dismounts at parallel bars

Hiro Hirabayayashi, Daisuke Takeshita

Affiliation: Department of Life Sciences (Sports Sciences), Graduate School of Arts and Sciences, University of Tokyo.

Address: The University of Tokyo, Building No. 9, 3-8-1 Komaba, Meguro-ku, Tokyo, 153-8902, Japan

Phone number: +81-3-5454-6133

Fax number: +81-3-5454-4317

Email: shiganai.hiro@gmail.com

KEYWORDS: Gymnastics, parallel bars, optimization, somersault, induced acceleration analysis

Word count: 2679

(intro: 310, method: 949, result: 523, discussion: 713, conclusion: 184)

Abstract

Backward somersault dismounts at parallel bars in artistic gymnastics are considered fundamental movements for other advanced skills, such as double backward tucked and piked somersaults. It has been previously discussed that angular momentum reduction around the center of mass occurs right before takeoff. However, such angular momentum reduction would decrease the number of rotations during somersaults, making it difficult for a gymnast to perform higher-valued dismounts. We hypothesized that avoiding this angular momentum reduction may be essential for enabling a large number of rotations and tested this hypothesis based on computer-based optimizations. We first determined the best stunt and observed hip flexion in the middle of the stunt, which is an unlikely movement for gymnasts. To avoid conclusions with applications only limited to unusual stunts with such hip flexion, we performed yet another optimization under additional constraints suppressing hip flexion in the middle of a stunt. In both these optimized stunts, angular momentum reduction was observed, thereby rejecting our hypothesis. However, an induced acceleration analysis of these stunts revealed that wrist and shoulder coordination weakened this angular momentum reduction, suggesting the importance of inter-joint coordination for better performance in backward somersault dismounts.

Introduction

Backward somersault dismounts at parallel bars in artistic gymnastics are considered fundamental movements for other advanced skills, such as double backward tucked and piked somersaults. (Fig. 1). A typical sequence of a backward somersault dismount at parallel bars begins with a still handstand on the parallel bars, followed by shoulder extension and takeoff from the parallel bars. However, gymnasts typically need to have an extended airtime and high angular momentum around the center of mass (CoM) for high-valued dismount skills.

A previous study has revealed that the horizontal and vertical momentum of the CoM decreases and increases, respectively, during the upward swing phase of a backward somersault dismount (Prassas and Papadopoulos 2001). They indicated that the force originating from parallel bars that induced the momentum change also reduced the angular momentum around the CoM. This was because the position of the CoM was higher and in front of the point of support.

However, this angular momentum reduction around the CoM could also reduce the number of rotations in the following backward somersault dismount because the number of rotations is proportional to the product of the airtime and angular momentum around the CoM. Such reduction in the number of rotations would make it more difficult for a gymnast to demonstrate high-valued dismount skills. Thus, we hypothesized that avoiding this angular momentum reduction during the upward swing phase is essential for somersault dismounts with higher number of rotations. To test this hypothesis, we conducted computer-based optimizations. We first determined the best stunt by maximizing the number of rotations via optimization and observed hip flexion in the middle of the stunt, which is not typical for gymnasts. To avoid conclusions that could only be applied to unusual stunts with hip flexion in the middle, we performed yet another optimization under additional constraints suppressing this hip flexion and tested the hypothesis by analyzing the two optimized results.

Method

Model Configuration

A two-dimensional model of a human and the parallel bars was developed to maximize the number of somersault rotations (Fig. 2). The human model comprised three segments representing the trunk, arms, and legs. The segments were connected at the wrist, shoulder, and hip joints. The wrist was assumed to be fixed on the parallel bars because gymnasts grasp parallel bars tightly with their hands. Further, the inertial parameters of the body were determined based on the body mass and the lengths of the body segments of a male gymnast (Ae et al. 1992). Notably, positive directions for the joint angles were assumed as follows: ulnar flexion for the wrist, extension for the shoulder, and flexion for the hip. All the angles were defined to be zero in the handstand position. Note that the origin of the displacement of parallel bars y_{PB} can be realized when no force is applied, including the gravitational force. In our model, each joint had a torque actuator that incorporated its physiological properties such as torque–angle and torque–angular velocity relationships. The torque of each actuator (τ_W, τ_S and τ_H) was determined based on the method proposed by Millard et al. (2019) (Fig. S-1). A linear spring and damper were used to represent the parallel bars (Linge et al. 2006).

A movement was simulated beginning from a still handstand, and a discrete time series of the active state for each joint with a 1/20 s resolution was used as the input. Cubic spline interpolation was used to obtain a time series with finer time resolution. The joint torque at each time was calculated considering the active states and the torque–angle–angular velocity relationships (Millard et al. 2019). The obtained joint torques were used to numerically integrate Newton's equations, and the angles and angular velocities were obtained (Fig. S-2). To identify the input yielding the best performance, an optimizing algorithm with genetic algorithms and simulated annealing was developed.

To quantify the performance of a simulated movement, the number of rotations N_r was defined as follows:

$$N_r = \frac{L_{CoM}|_{takeoff}}{2\pi I_{stretched}} T_{air}, \tag{1}$$

where $L_{CoM}|_{takeoff}$ denotes the angular momentum around the CoM at takeoff, $I_{stretched}$ denotes the moment of inertia for the stretched posture, and T_{air} denotes the airtime. The takeoff occurred when the displacement of the parallel bars y_{PB} was equal to zero and $\theta_{Body} > 180°$, where $\theta_{Body} := \theta_W + \theta_S$. Here, T_{air} is defined as the time when the CoM approaches the height of the CoM in a standing position on the ground that is 1.8 m below the parallel bars. The stretched posture is also defined as a standing position ($\theta_S = 180°$ and $\theta_H = 0°$).

Here, N_r is a suitable indicator of performance for the following two reasons: (1) larger N_r values enable gymnasts to perform more difficult backward dismounts, and (2) when they perform tucked or piked dismounts, gymnasts can prepare for a suitable landing with larger N_r values by stretching their bodies before landing, which requires extra rotations.

Two conditions were defined for successful movements: (1) $|\theta_W| < 45°$ all the time, which otherwise was considered out of balance, and (2) $y_{PB} < 0$ all the time because otherwise the parallel bars vibrated quickly and became unrealistic. The integration of Newton's equations of motion was terminated when the simulated movement surpassed either of the two conditions.

Two optimizing conditions were also defined: (1) unconstrained condition using the aforementioned method and (2) hip-flexion suppressed condition, which yields an additional condition. The additional condition was $\theta_H < 0$ all the time while $\theta_{Body} < 180°$. The hip-flexion suppressed condition was used because we observed, in the best stunt of the unconstrained condition, hip flexion in the middle of the stunt, which actual gymnasts do not usually perform, and thus sought for an optimized stunt without such hip flexion. In the figure legends, we denote the unconstrained condition as "Uncon" and the hip-flexion suppressed condition as "HFS."

Contribution of joint torques to physical quantities

The contribution of joint torques to L_{CoM} and other physical quantities was analyzed, as previously reported (Liu et al. 2006, Zajac et al. 2002, Hirashima 2011, Koike et al. 2019).

Notably, the generalized acceleration, including translational and angular acceleration, can be expressed based on a linear combination of generalized forces, including forces and torques. For example, the angular acceleration of the wrist joint (α_W) can be expressed as

$$\alpha_W = A_{\alpha_W}^{\tau_W}\tau_W + A_{\alpha_W}^{\tau_S}\tau_S + A_{\alpha_W}^{\tau_H}\tau_H + A_{\alpha_W}^{F_{PB}}F_{PB} + C_{\alpha_W} \tag{2}$$

$$(= \alpha_W^{\tau_W} + \alpha_W^{\tau_S} + \alpha_W^{\tau_H} + \alpha_W^{F_{PB}} + C_{\alpha_W}), \tag{3}$$

where $A_{\alpha_W}^{\tau_W}, A_{\alpha_W}^{\tau_S}, A_{\alpha_W}^{\tau_H}, A_{\alpha_W}^{F_{PB}}$, and C_{α_W} are coefficients that do not involve generalized forces (τ_W, τ_S, τ_H, or F_{PB}). $\alpha_W^{\tau_W} (= A_{\alpha_W}^{\tau_W}\tau_W)$ can be defined as the contribution of τ_W to α_W, and $\alpha_W^{\tau_S}, \alpha_W^{\tau_H}$, and $\alpha_W^{F_{PB}}$ can be defined similarly. C_{α_W} contains effects that are independent of joint torques and F_{PB} such as those of the gravitational force and inertia. The angular acceleration of the shoulder and hip joints (α_S and α_H) and the acceleration of parallel bars (a_{PB}) can be expressed similarly.

For the x coordinate of the CoM (x_{CoM}), the equation of motion is

$$Ma_{x_{CoM}} = F_x, \tag{4}$$

where $a_{x_{CoM}}$ denotes the horizontal acceleration of the CoM, and F_x denotes the horizontal force originating from the parallel bars and acting on the upper limb (Fig. 2b). As $x_{CoM} = x_{CoM}(\theta_W, \theta_S, \theta_H, y_{PB})$,

$$a_{x_{CoM}} = c_W\alpha_W + c_S\alpha_S + c_H\alpha_H + c_{PB}a_{PB} + d, \tag{5}$$

where c_W, c_S, c_H, c_{PB}, and d are coefficients that do not involve generalized accelerations. Therefore, from Equations 2–5,

$$F_x = A_{F_x}^{\tau_W}\tau_W + A_{F_x}^{\tau_S}\tau_S + A_{F_x}^{\tau_H}\tau_H + A_{F_x}^{F_{PB}}F_{PB} + C_{F_x} \tag{6}$$

$$(= F_x^{\tau_W} + F_x^{\tau_S} + F_x^{\tau_H} + F_x^{F_{PB}} + C_{F_x}), \tag{7}$$

where $A_{F_x}^{\tau_W}, A_{F_x}^{\tau_S}, A_{F_x}^{\tau_H}, A_{F_x}^{F_{PB}}$, and C_{F_x} are coefficients that do not involve generalized forces. $F_x^{\tau_W}(= A_{F_x}^{\tau_W}\tau_W)$ is defined as the contribution of τ_W to F_x, and $F_x^{\tau_S}, F_x^{\tau_H}$, and $F_x^{F_{PB}}$ are defined similarly. C_{F_x} contains effects that are independent of joint torques and F_{PB} such as those of the gravitational force and inertia. From the equation of motion for the y coordinate of the CoM (y_{CoM}), the vertical force F_y originating from the parallel bars and acting on the upper limb can be calculated similarly:

$$F_y = A_{F_y}^{\tau_W}\tau_W + A_{F_y}^{\tau_S}\tau_S + A_{F_y}^{\tau_H}\tau_H + A_{F_y}^{F_{PB}}F_{PB} + C_{F_y} \tag{8}$$

$$(= F_y^{\tau_W} + F_y^{\tau_S} + F_y^{\tau_H} + F_y^{F_{PB}} + C_{F_y}), \tag{9}$$

where $A_{F_y}^{\tau_W}, A_{F_y}^{\tau_S}, A_{F_y}^{\tau_H}, A_{F_y}^{F_{PB}}$, and C_{F_y} are coefficients that do not involve generalized forces. $F_y^{\tau_W}(= A_{F_y}^{\tau_W}\tau_W)$ is defined as the contribution of τ_W to F_y, and $F_y^{\tau_S}, F_y^{\tau_H}$, and $F_y^{F_{PB}}$ are defined similarly. C_{F_y} contains effects that are independent of joint torques and F_{PB} such as those of the gravitational force and inertia.

L_{CoM} satisfies the following equation:

$$\begin{aligned}\frac{dL_{CoM}}{dt} &= (\vec{p_W} - \vec{p_G}) \times \vec{F} + \tau_W \\ &= (y_{CoM} - y_{PB})F_x - x_{CoM}F_y + \tau_W \end{aligned} \tag{10}$$

where $\vec{p_G}$ and $\vec{p_W}$ denote the position vectors of the CoM and wrist joint, respectively, and $\vec{F}(= [F_x, F_y]^T)$ represents the external force vector at the wrist joint (Fig. S-3, 2b). Therefore, from Equation 6–10,

$$\frac{dL_{CoM}}{dt} = A_{dL_{CoM}}^{\tau_W}\tau_W + A_{dL_{CoM}}^{\tau_S}\tau_S + A_{dL_{CoM}}^{\tau_H}\tau_H + A_{dL_{CoM}}^{F_{PB}}F_{PB} + C_{dL_{CoM}}, \tag{11}$$

where $A_{dL_{CoM}}^{\tau_W}, A_{dL_{CoM}}^{\tau_S}, A_{dL_{CoM}}^{\tau_H}, A_{dL_{CoM}}^{F_{PB}}$, and $C_{dL_{CoM}}$ are coefficients that do not involve τ_W, τ_S, τ_H, or F_{PB}. $A_{dL_{CoM}}^{\tau_W}\tau_W$ is defined as the contribution of τ_W to the torque around the CoM, and $A_{dL_{CoM}}^{\tau_S}\tau_S, A_{dL_{CoM}}^{\tau_H}\tau_H$, and $F_y^{F_{PB}}$ are defined similarly. $C_{dL_{CoM}}$ contains effects that are independent of joint torques and F_{PB} such as those of the gravitational force and inertia.

Result

The performance of the optimized movements in both conditions was sufficiently significant to perform the triple backward piked somersault (Fig. 3). This indicates successful optimization, given that the most successful backward somersault dismount by real gymnasts is the double backward piked somersault (Fig. 1d).

The number of rotations in the unconstrained condition was larger than that in the hip-flexion suppressed condition (Table 1). This was expected as all the movements satisfying the hip-flexion suppressed condition also satisfy the unconstrained condition. Although T_{air} in the unconstrained condition was shorter than that in the hip-flexion suppressed condition, the number of rotations was larger in the unconstrained condition because of its larger rotational velocity.

The number of rotations was positively correlated with $L_{CoM}|_{takeoff}$ but negatively correlated with T_{air} (Fig. 4), suggesting that increasing the $L_{CoM}|_{takeoff}$ was more crucial for increasing the number of rotations than increasing T_{air}. This indicates the necessity of avoiding the reduction of L_{CoM} for a large number of rotations.

In the following description, time intervals are denoted by $[s,\ t]$, where s and t denote time points before takeoff. For example, $[-0.4\,\mathrm{s},\ -0.2\,\mathrm{s}]$ represents the time interval from 0.4 s to 0.2 s before the takeoff.

The wrist and shoulder angles (θ_W and θ_S) and the displacement of parallel bars (y_{PB}) were quite similar in both conditions, whereas the hip angle (θ_H) in the unconstrained condition was remarkably larger than that in the hip–flexion suppressed condition (Fig. 5). θ_H in the unconstrained condition was positive at $[-0.4\,\mathrm{s},\ -0.2\,\mathrm{s}]$ in the middle of the downward phase. We refer to this movement as the "hip flexion," which any gymnast is unlikely to perform.

With regard to the active states, the wrist and shoulder active states demonstrated a similar pattern in both conditions; the wrist active state was maintained at around 1 before $-0.8\,\mathrm{s}$, whereas the shoulder active state was maintained at around 1 after $-0.8\,\mathrm{s}$ (Fig. 5). The hip active states in both conditions were not similar, especially at $[-0.6\,\mathrm{s}, -0.4\,\mathrm{s}]$; the hip active state in the unconstrained condition rose up earlier than that in hip-flexion suppressed condition. It appears that this earlier rise of the hip active state caused hip flexion in the middle of the downward phase.

The changes in L_{CoM} in both conditions were similar to each other; it increased right after $-0.8\,\mathrm{s}$ and decreased after $-0.1\,\mathrm{s}$ (Fig. 6). This reduction is similar to that in a previous study (Prassas and Papadopoulos 2001). We refer to this reduction of L_{CoM} after $-0.1\,\mathrm{s}$ as the "brake effect." Therefore, our hypothesis that claimed the necessity of avoiding L_{CoM} reduction for a large number of rotations was rejected.

We decomposed the torque around the CoM in $[-0.1\,\mathrm{s}, 0\,\mathrm{s}]$ based on Equation 10 to examine the reason for the brake effect; while τ_W was always positive, the other two terms, $(y_{CoM} - y_{PB})F_x$ and $-x_{CoM}F_y$, were mostly negative (Fig. 7a). These negative torques around the CoM were also consistent with that in the previous study (Prassas and Papadopoulos 2001). We further decomposed $(y_{CoM} - y_{PB})F_x$ into $y_{CoM} - y_{PB}$ and F_x, and $-x_{CoM}F_y$ into x_{CoM} and F_y. (Fig. 7b, 7c). $(y_{CoM} - y_{PB})F_x$ was negative at $[-0.1\,\mathrm{s}, 0\,\mathrm{s}]$ because $(y_{CoM} - y_{PB})$ remained positive and F_x turned negative at $-0.15\,\mathrm{s}$, and $-x_{CoM}F_y$ was negative because F_y remained positive and x_{CoM} turned positive at $-0.1\,\mathrm{s}$. The main cause of the brake effect was $(y_{CoM} - y_{PB})F_x$ with respect to the magnitude.

Discussion

In this study, we conducted computer-based optimization of backward somersault dismount at parallel bars to test the hypothesis that avoiding the brake effect is required for a large number of rotations. In both the optimized stunts, the brake effect was observed, rejecting our hypothesis. However, we propose that, in these two optimized stunts, the brake effect is minimized via the coordination between the wrist and shoulder joints, suggesting the importance of weakening the brake effect.

Considering Equation 10, the brake effect could be weakened via four approaches: (1) decreasing $y_{CoM} - y_{PB}$, (2) decreasing F_y, (3) increasing F_x, and (4) decreasing x_{CoM}. However, we argue that (1), (2), and (3) are not effective in weakening the brake effect for a large number of rotations, whereas (4) is effective.

In (1), the rise of $y_{CoM} - y_{PB}$ in the upward swing phase is quite important to gain T_{air}, since it determines the vertical CoM velocity at takeoff. The rise of $y_{CoM} - y_{PB}$ also gains CoM height at takeoff, which would increase T_{air}. Thus, decreasing $y_{CoM} - y_{PB}$ to weaken the brake effect would reduce T_{air}; therefore, we assume that decreasing $y_{CoM} - y_{PB}$ is not effective to weaken the brake effect.

As regards (2), decreasing F_y would also reduce T_{air}, which may reduce the number of rotations.

With regard to (3), increasing F_x is not effective either, because increasing F_x would also decrease F_y, as discussed below. First, F_x is proportional to $-F_y$ in $[-0.1\,\mathrm{s}, 0\,\mathrm{s}]$. This holds because F_x and F_y in $[-0.1\,\mathrm{s}, 0\,\mathrm{s}]$ are almost equal to $F_x^{F_{PB}}$ and $F_y^{F_{PB}}$, respectively (Fig. S-4). This approximation holds because the effect of large F_{PB} by large $|y_{PB}|$ surpasses the effect of other terms. Therefore,

$$\frac{F_x}{F_y} \approx \frac{A_{F_x}^{F_{PB}}}{A_{F_y}^{F_{PB}}} \tag{12}$$

$$\because F_x \approx F_x^{F_{PB}} = A_{F_x}^{F_{PB}} F_{PB},\ F_y \approx F_y^{F_{PB}} = A_{F_y}^{F_{PB}} F_{PB} \tag{13}$$

$$\therefore F_x \propto F_y \tag{14}$$

Furthermore, because $F_x/F_y < 0$ in $[-0.15\,\mathrm{s},\ 0\,\mathrm{s}]$, $A_{F_x}^{F_{PB}}/A_{F_y}^{F_{PB}} < 0$ in $[-0.15\,\mathrm{s},\ 0\,\mathrm{s}]$. This indicates that increasing F_x would also reduce F_y, which would in turn reduce T_{air}.

As regards (4), x_{CoM} can be reduced by generating a negative F_x before the occurrence of the brake effect, and its cumulative effect in reducing x_{CoM} is more significant when a negative F_x is generated as early as possible. According to Fig. 8, τ_W generated a negative F_x before $-0.8\,\mathrm{s}$, and τ_S generated a positive F_x after $-0.8\,\mathrm{s}$, which was suitable considering the cumulative effect.

However, a negative F_x would also reduce L_{CoM}, as $y_{CoM} - y_{PB} > 0$ (Equation 10). This indicates that τ_W reduced the brake effect by reducing x_{CoM} while reducing L_{CoM} with a negative F_x, and τ_S generated L_{CoM} with a positive F_x (Fig. 8). This coordination pattern of τ_W and τ_S was caused by a unique feature of τ_W discussed below.

The effect of generating a negative F_x via joint torques on L_{CoM} can be evaluated by

$$\frac{A_{dL_{CoM}}^{\tau_{(\cdot)}}}{A_{F_x}^{\tau_{(\cdot)}}} \left(= \frac{A_{dL_{CoM}}^{\tau_{(\cdot)}} \tau_{(\cdot)}}{A_{F_x}^{\tau_{(\cdot)}} \tau_{(\cdot)}} = \frac{dL_{CoM}^{\tau_{(\cdot)}}}{F_x^{\tau_{(\cdot)}}} \right). \tag{15}$$

Reduction in $dL_{CoM}^{\tau_{(\cdot)}}$ due to a negative $F_x^{\tau_{(\cdot)}}$ is smaller for smaller $A_{dL_{CoM}}^{\tau_{(\cdot)}}/A_{F_x}^{\tau_{(\cdot)}}$

because

$$dL_{CoM}^{\tau(\cdot)} = \frac{A_{dL_{CoM}}^{\tau(\cdot)}}{A_{F_x}^{\tau(\cdot)}} F_x^{\tau(\cdot)} = -\frac{A_{dL_{CoM}}^{\tau(\cdot)}}{A_{F_x}^{\tau(\cdot)}} | - F_x^{\tau(\cdot)} |. \tag{16}$$

According to Fig. 9a, $A_{dL_{CoM}}^{\tau_W}/A_{F_x}^{\tau_W}$ is smaller than $A_{dL_{CoM}}^{\tau_S}/A_{F_x}^{\tau_S}$ (note that $A_{dL_{CoM}}^{\tau_H}/A_{F_x}^{\tau_H}$ is remarkably similar to $A_{dL_{CoM}}^{\tau_S}/A_{F_x}^{\tau_S}$, although it is not plotted herein). This indicates that generating a negative F_x with τ_W is the best strategy to reduce x_{CoM} with less L_{CoM} reduction.

This unique feature of τ_W is attributable to the fact that the wrist joint is fixed on the parallel bars while neither the shoulder nor the hip joint has such a constraint. To clarify the difference, the torque around the CoM generated by τ_S is given as (Equation 10):

$$\begin{aligned}(y_{CoM} - y_{PB})F_x^{\tau_S} - x_{CoM}F_y^{\tau_S} &= \left[(y_{CoM} - y_{PB})A_{F_x}^{\tau_S} - x_{CoM}A_{F_y}^{\tau_S}\right]\tau_S \\ &= A_{dL_{CoM}}^{\tau_S}\tau_S. \end{aligned}\tag{17}$$

As $-x_{CoM}A_{F_y}^{\tau_S}$ is sufficiently small compared with $(y_{CoM} - y_{PB})A_{F_x}^{\tau_S}$ (Fig. 9b), the following approximation holds:

$$\frac{A_{dL_{CoM}}^{\tau_S}}{A_{F_x}^{\tau_S}} \approx y_{CoM} - y_{PB}. \tag{18}$$

The same holds for τ_H (data not shown). In contrast, because the wrist joint is fixed on the parallel bars, the torque around the CoM generated by τ_W is as follows:

$$\begin{aligned}&(y_{CoM} - y_{PB})F_x^{\tau_W} - x_{CoM}F_y^{\tau_W} + \tau_W \\ &\qquad = \left[(y_{CoM} - y_{PB})A_{F_x}^{\tau_W} - x_{CoM}A_{F_y}^{\tau_W} + 1\right]\tau_W \\ &\qquad = A_{dL_{CoM}}^{\tau_W}\tau_W. \end{aligned}\tag{19}$$

As $-x_{CoM}A^{\tau_W}_{F_y}$ is extremely small (data not shown), the following approximation holds:

$$\frac{A^{\tau_W}_{dL_{CoM}}}{A^{\tau_W}_{F_x}} \approx y_{CoM} - y_{PB} + \frac{1}{A^{\tau_W}_{F_x}} \tag{20}$$

Furthermore, because $A^{\tau_W}_{F_x}$ is negative (Fig. 9c), the following inequality holds:

$$\frac{A^{\tau_W}_{dL_{CoM}}}{A^{\tau_W}_{F_x}} - \frac{A^{\tau_S}_{dL_{CoM}}}{A^{\tau_S}_{F_x}} \approx \frac{1}{A^{\tau_W}_{F_x}} < 0, \tag{21}$$

$$\therefore \frac{A^{\tau_W}_{dL_{CoM}}}{A^{\tau_W}_{F_x}} < \frac{A^{\tau_S}_{dL_{CoM}}}{A^{\tau_S}_{F_x}}. \tag{22}$$

Therefore, τ_W can generate a negative F_x with a lower L_{CoM} reduction than τ_S or τ_H. Owing to this feature, τ_W before -0.8 s can successfully reduce x_{CoM} to weaken the brake effect considering x_{CoM} decreased before -0.8 s (Fig. S-5).

Alternatively, $A^{\tau_S}_{dL_{CoM}}/A^{\tau_S}_{F_x}$ and $A^{\tau_H}_{dL_{CoM}}/A^{\tau_H}_{F_x}$ are larger than $A^{\tau_W}_{dL_{CoM}}/A^{\tau_W}_{F_x}$. This implies that τ_S and τ_H can generate a certain amount of L_{CoM} with a less positive F_x than τ_W. A reduction in the positive F_x would also reduce x_{CoM}, resulting in weakening of the brake effect. Furthermore, because $A^{\tau_H}_{dL_{CoM}}$ is extremely small compared with the other terms (Fig. 9d), generating a torque around the CoM via τ_S would be more effective than generating it via τ_H after -0.8 s.

In summary, the coordination between the wrist and shoulder joint appears to be a strategy for generating L_{CoM} while reducing the brake effect. The wrist first generates a negative F_x, and the shoulder then generates a positive F_x to effectively reduce the value of x_{CoM} considering the cumulative effect. The wrist generates a negative F_x because it generates the least L_{CoM} reduction with a negative F_x, and the shoulder generates a positive F_x because it generates the largest L_{CoM} production with a positive F_x.

CONCLUSION

The aim of this study was to test the hypothesis that avoiding the reduction of angular momentum around the CoM right before takeoff is required for a large number of rotations in backward somersault dismount at parallel bars. We performed computer-based optimization and observed the reduction of angular momentum in optimized stunts, rejecting our hypothesis. However, we found that wrist and shoulder torques were activated in order, and an induced acceleration analysis revealed that this coordination weakens the reduction of the angular momentum.

However, the reason why either of the optimized stunts did not completely avoid the reduction of angular momentum around CoM is unclear. In the optimized stunts, the angular momentum was mainly reduced by the negative horizontal force from the parallel bars (Fig. 7). Since the negative horizontal force was proportional to the positive vertical force (Equation 14), decreasing the magnitude of the negative horizontal for larger angular momentum would have decreased the positive vertical force, thereby decreasing the airtime. Thus, our future task involves identifying the tradeoff between the angular momentum and airtime caused by the forces from the parallel bars.

ACKNOWLEDGMENTS

This work was partially supported by JSPS KAKENHI Grant Number JP20K11330. We also would like to thank the members of the Sports Biomechanics Lab at the University of Tokyo for helpful discussions. We would like to thank Editage (www.editage.com) for English language editing.

Declaration of Competing Interest

The authors declare that they have no known competing financial interests or personal relationships that could have appeared to influence the work reported in this paper.

References

Ae, M., Tang, H., Yokoi, T., 1992. Estimation of inertia properties of the body segments in japanese athletes. Biomechanisms 11, 23–33.

Hirashima, M., 2011. Induced acceleration analysis of three-dimensional multi-joint movements and its application to sports movements. In: Klika, V., Theoretical Biomechanics, IntechOpen, Rijeka, chapter 14.

Koike, S., Ishikawa, T., Willmott, A. P., Bezodis, N. E., 2019. Direct and indirect effects of joint torque inputs during an induced speed analysis of a swinging motion. Journal of Biomechanics 86, 8–16.

Linge, S., Hallingstad, O., Solberg, F., 2006. Modelling the parallel bars in men ' s artistic gymnastics. Human Movement Science 25(2), 221–237.

Liu, M. Q., Anderson, F. C., Pandy, M. G., Delp, S. L., 2006. Muscles that support the body also modulate forward progression during walking. Journal of Biomechanics 39(14), 2623–2630.

Millard, M., Emonds, A. L., Harant, M., Mombaur, K., 2019. A reduced muscle model and planar musculoskeletal model fit for the simulation of whole-body movements. Journal of Biomechanics 89, 11–20.

Prassas, S., Papadopoulos, C., 2001. Mechanics of forward support swing skills on the parallel bars. Journal of Human Movement Studies 40, 335–350.

Zajac, F. E., Neptune, R. R., Kautz, S. A., 2002. Biomechanics and muscle coordination of human walking: Part i: Introduction to concepts, power transfer, dynamics and simulations. Gait & Posture 16(3), 215–232.

Table 1: Best performances in the two conditions following Equation 1. Note that rotational velocity is equal to $\frac{L_{CoM}|_{takeoff}}{2\times\pi\times I_{stretched}}$.

Condition	Number of rotations	Rotational velocity [s^{-1}]	Airtime [s]
Unconstrained	1.26	1.46	0.856
Hip–flexion suppressed	1.22	1.40	0.871

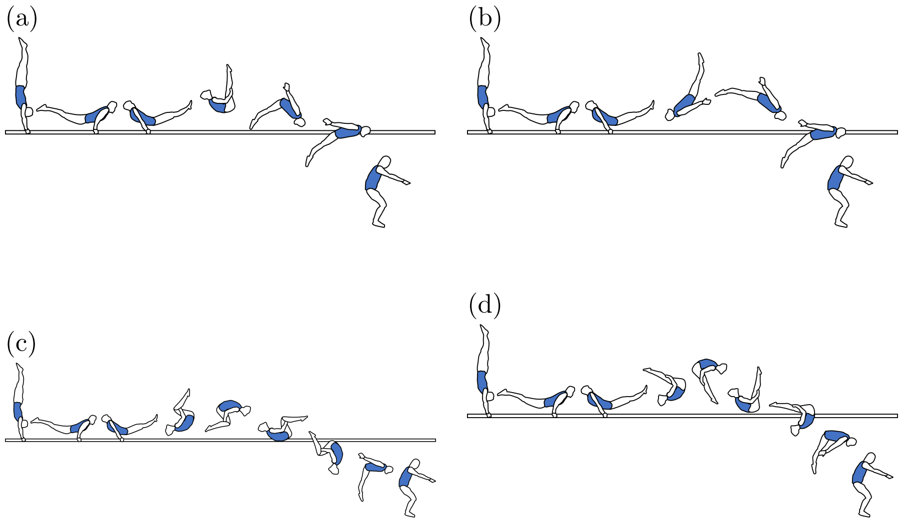

Figure 1: Examples of backward somersault dismounts in the order of their difficulty. (a) Single backward piked somersault (the easiest). (b) Single backward stretched somersault. (c) Double backward tucked somersault. (d) Double backward piked somersault (the most difficult). For any of the backward dismounts, the gymnasts begin with handstands and swing down their entire body until takeoff while supporting their body above the parallel bars. The moment of inertia decreases in the order of the stretched, piked, and tucked postures. The difficulty is evaluated by combining the moment of inertia and the number of rotations. Although the moment of inertia in the tucked posture is smaller than that in the stretched posture, the difficulty corresponding to (c) is greater than that corresponding to (b) because the number of rotations is larger in (c). (d) is the most difficult dismount among the backward dismounts performed by real gymnasts.

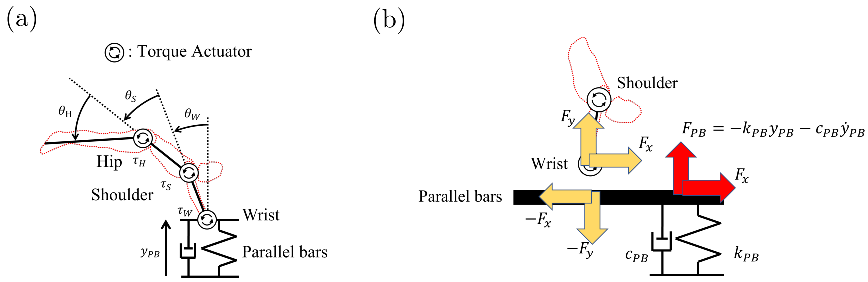

Figure 2: Illustration of simulated model parameters and external forces acting on the gymnast. (a): Simulated model. The model consists of a gymnast and parallel bars. The gymnast is modeled as three linked segments with the wrist, shoulder, and hip joints. Each joint has a torque actuator with its physiological characteristics. The parallel bars are modeled using a linear spring and damper. The angles of all the joints $(\theta_W, \theta_S, \theta_H)$ are defined, with zeros corresponding to the handstand posture. The positives are considered in ulnar flexion for the wrist, extension for the shoulder, and flexion for the hip. (b): Definition of F_{PB}, F_x, and F_y. Note that F_{PB} is a vertical force acting from the spring-damper element to the parallel bars, and F_x and F_y are the horizontal and vertical forces acting from the parallel bars to the wrist joint, respectively. F_y does not always match with F_{PB} because the parallel bars have mass and vertical acceleration.

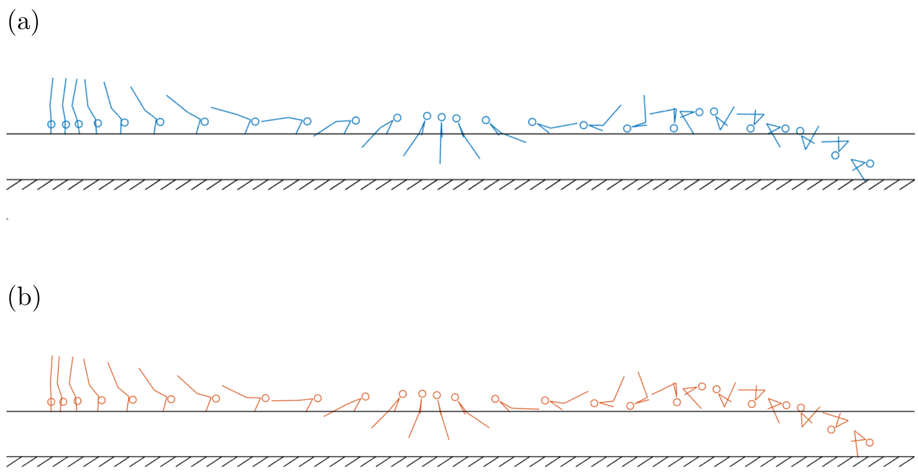

Figure 3: Simulated performance of the optimization results in the piked posture to compare the difficulty with that shown in Fig. 1d. (a) Best performance in the unconstrained condition in the piked posture. (b) Best performance in the hip-flexion suppressed condition in the piked posture. Both performances qualified the triple backward piked somersault dismount. (a) was better than (b) because (a) had enough rotation to stretch the body to prepare for landing while (b) did not have enough rotation to stretch the body for landing.

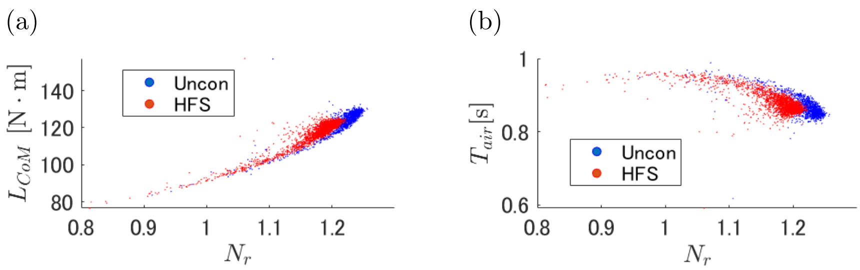

Figure 4: (a) N_r vs. $L_{CoM}|_{takeoff}$. (b) N_r vs. T_{air}. The results whose $N_r > 0.8$ found in the two optimizations were plotted.

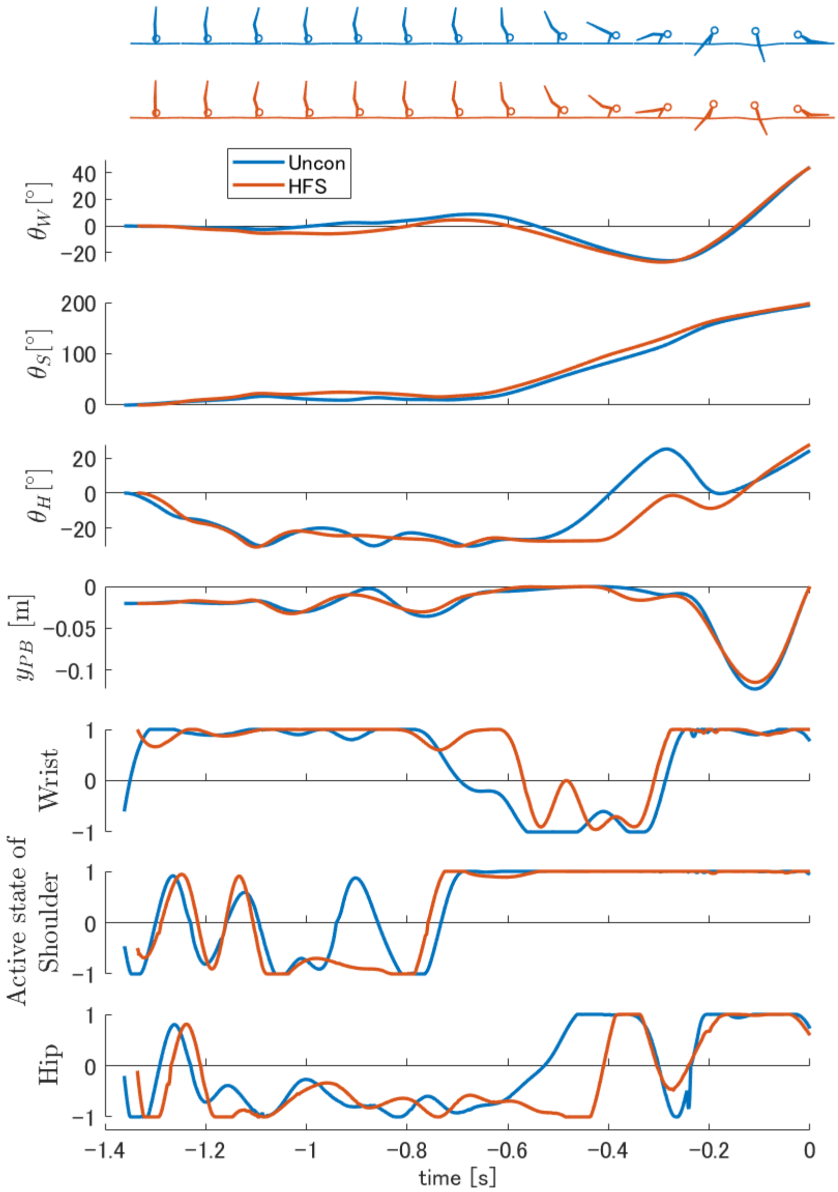

Figure 5: Relevant kinematic variables and active states of each joint: from the top, joint angles of the wrist, shoulder, and hip, displacement of the parallel bars, and active states of the wrist, shoulder, and hip in the unconstrained (blue) and the hip-flexion suppressed (red) conditions.

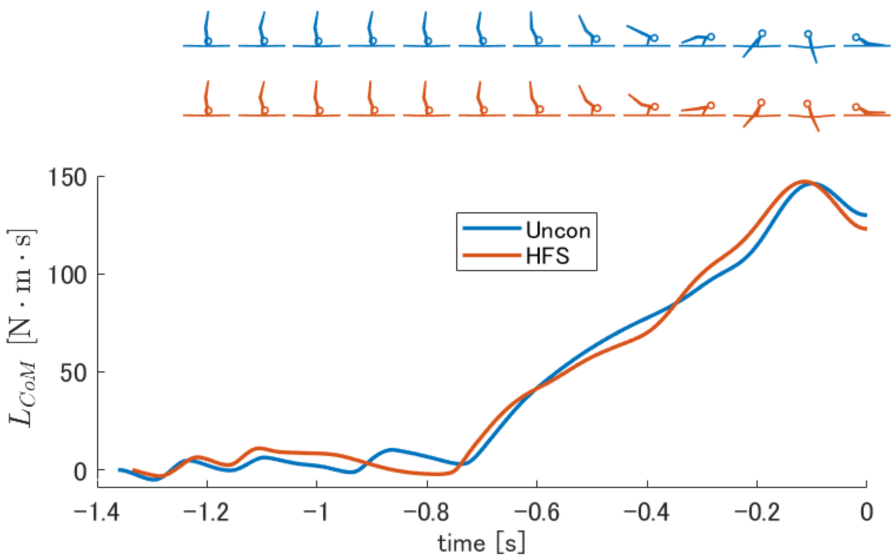

Figure 6: Angular momentum around the CoM (L_{CoM}) in the unconstrained (blue) and the hip-flexion suppressed (red) conditions.

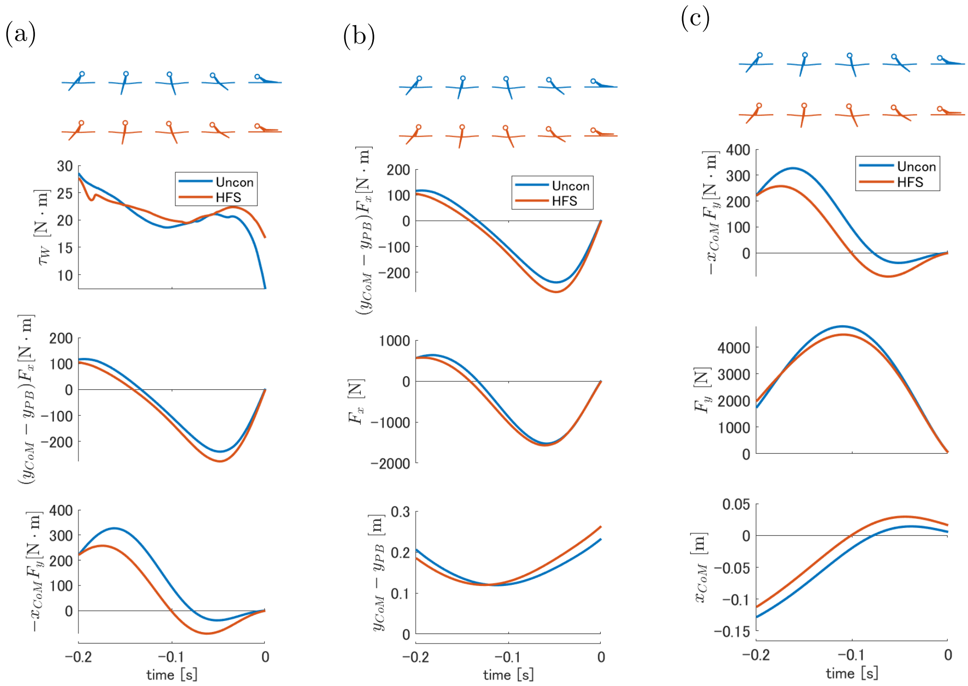

Figure 7: Analysis of the brake effect. (a): Decomposition of torque around the CoM based on Equation 10. From the top, τ_W, $(y_{CoM} - y_{PB})F_x$, and $-x_{CoM}F_y$ are presented. The positive value corresponds to increasing L_{CoM}. (b): Decomposition of $(y_{CoM} - y_{PB})F_x$ into F_x and $y_{CoM} - y_{PB}$. From the top, $(y_{CoM} - y_{PB})F_x$, F_x, and $y_{CoM} - y_{PB}$ are presented. (c): Decomposition of $-x_{CoM}F_y$ into F_y and x_{CoM}. From the top, $-x_{CoM}F_y$, F_y, and x_{CoM} are illustrated.

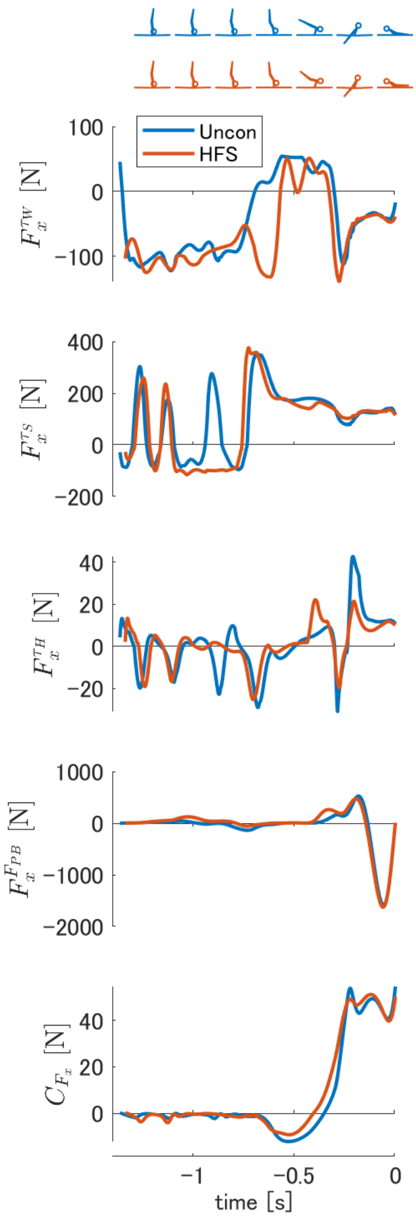

Figure 8: Breakdown of F_x into the contributions of the wrist, shoulder, and hip torques, as well as F_{PB}, and C_{F_x}.

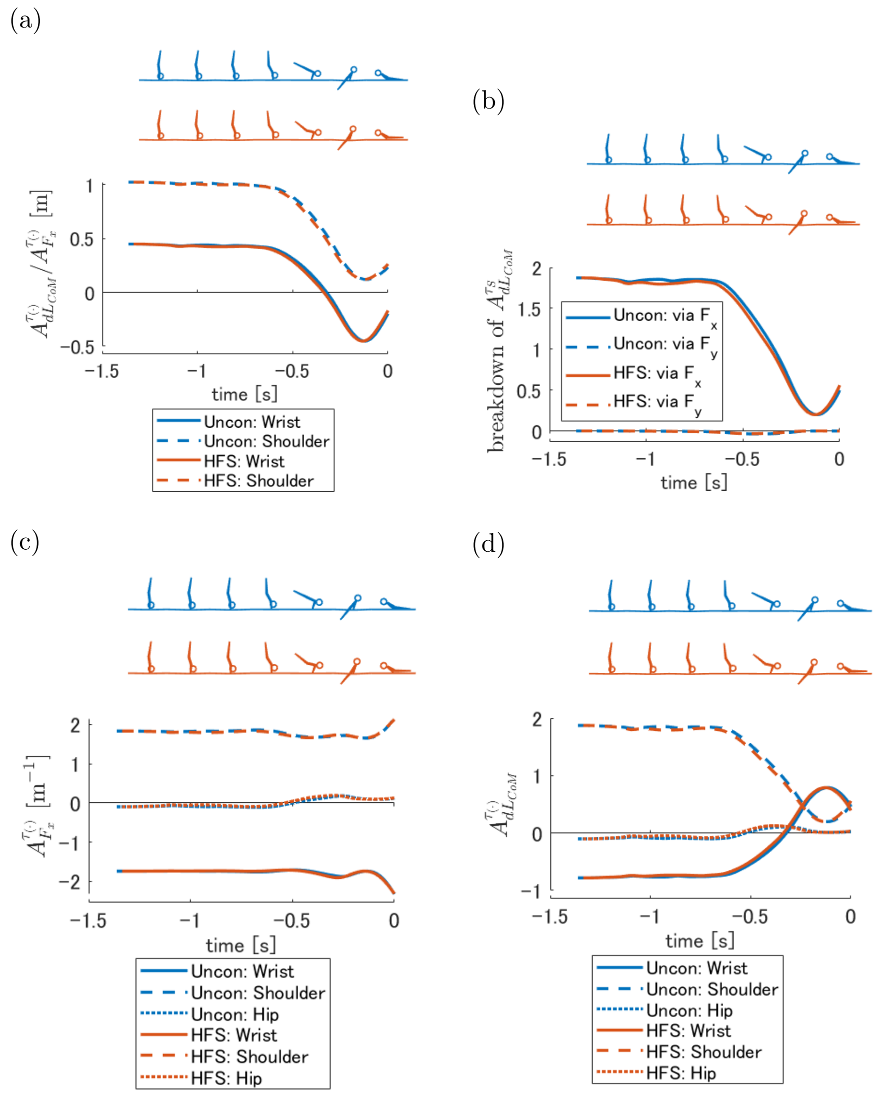

Figure 9: (a): Ratio of the coefficients of contribution to the torque around the CoM ($= A^{\tau_{(\cdot)}}_{dL_{CoM}}$) to F_x ($= A^{\tau_{(\cdot)}}_{F_x}$). The larger the value, the lower the magnitude of F_x that needs to be generated to gain a certain amount of torque around the CoM. (b): Breakdown of $A^{\tau_S}_{dL_{CoM}}$ into terms via F_x and F_y. Note that the terms obtained via F_x are equal to $(y_{CoM} - y_{PB})A^{\tau_S}_{F_x}$, and the terms obtained via F_y are equal to $-x_{CoM}A^{\tau_S}_{F_y}$. (c): Coefficients of the contributions of the wrist, shoulder, and hip torques to F_x . (d): Coefficients of the contributions of the wrist, shoulder, and hip to the torque around the CoM ($= dL_{CoM}$).

Supplementary Figures

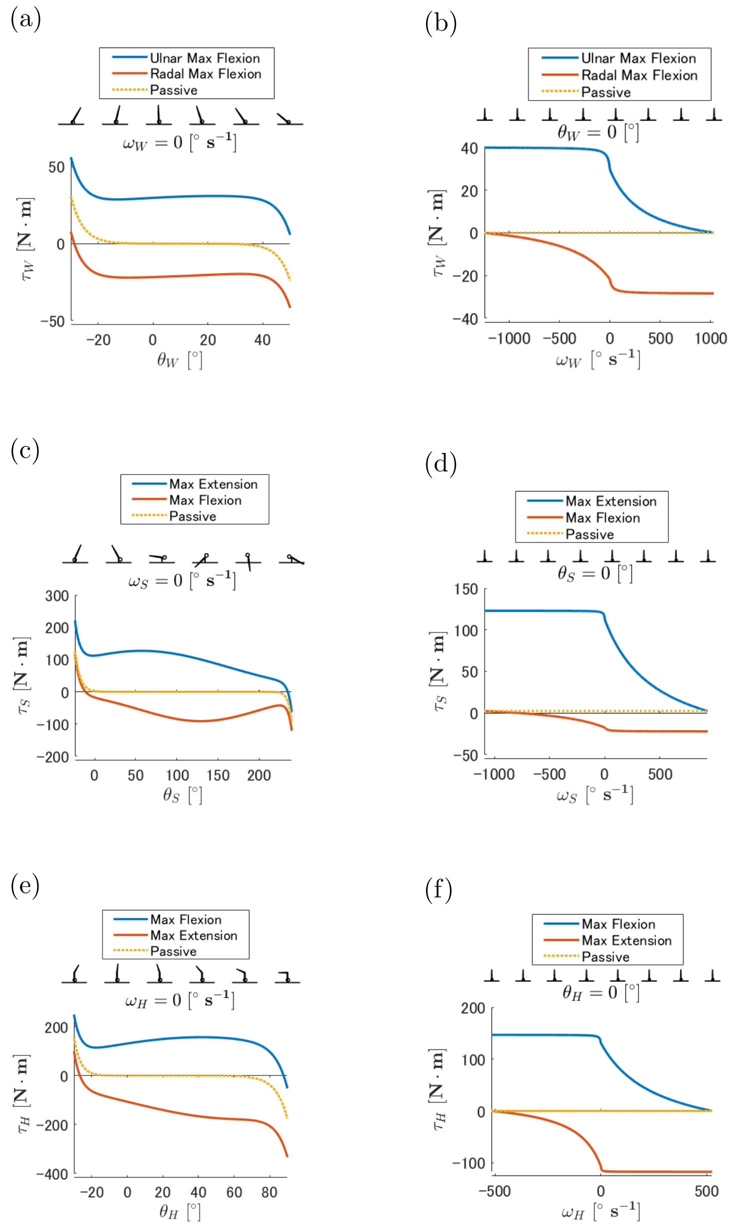

Figure S-1: Physiological properties incorporated into the toque actuators. (S-1a), (S-1c), (S-1e) Torque–angle relationship for the wrist, shoulder, and hip, respectively. (S-1b), (S-1d), (S-1f) Torque–angular velocity relationship for the wrist, shoulder, and hip, respectively. The torque–angle relationships do not affect τ significantly when θ is far from the edge of the motion range. The torque–angular velocity relationships also do not affect τ significantly under eccentric ω. However, they change τ significantly under concentric ω

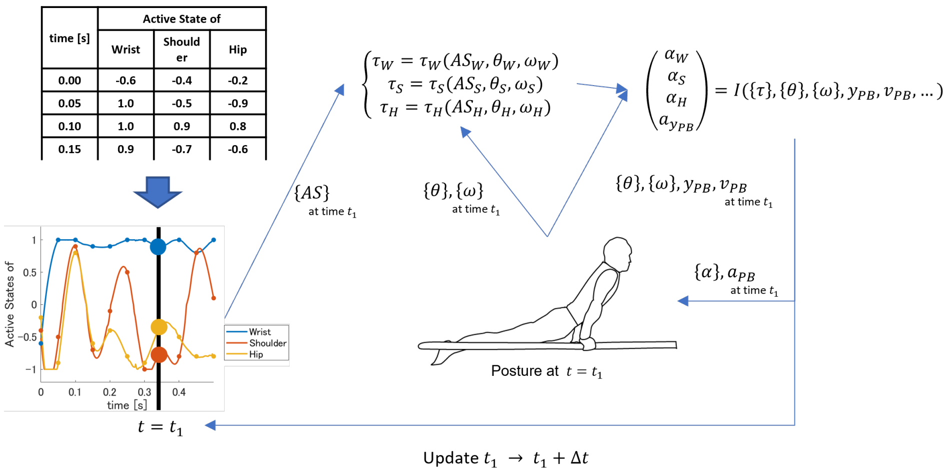

Figure S-2: Simulation Flow. A time series of the active state for each joint with a 1/20 s resolution is used as input (upper left). Cubic spline interpolation is used to obtain a time series (lower left). To simulate the state at $t = t_1$, the joint torque (τ) for each joint is calculated considering the active states and the torque–angle–angular velocity relationships with θ and ω (top middle). The obtained joint torques are used for numerically integrating Newton's Equations, and the angles and angular velocities are obtained.

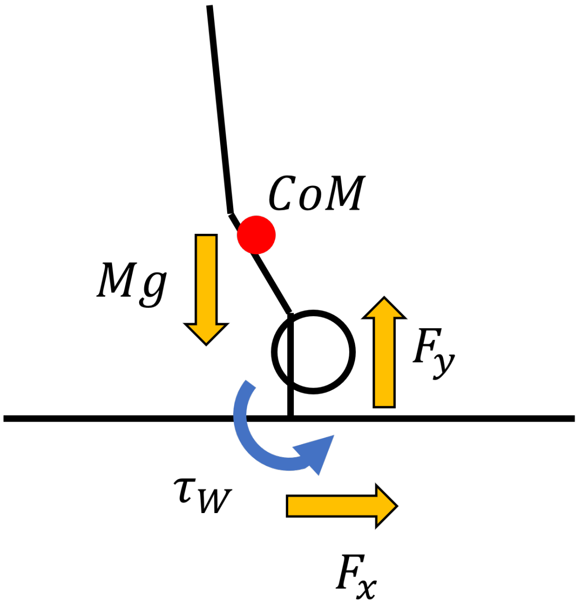

Figure S-3: The external forces and torque that affect L_{CoM} are displayed. The gravity acting on the gymnast does not affect L_{CoM} because the gravity applies to the CoM, thus creating no torque around the CoM. F_x and F_y affect L_{CoM} with a non-zero moment arm, and τ_W directly affects L_{CoM}.

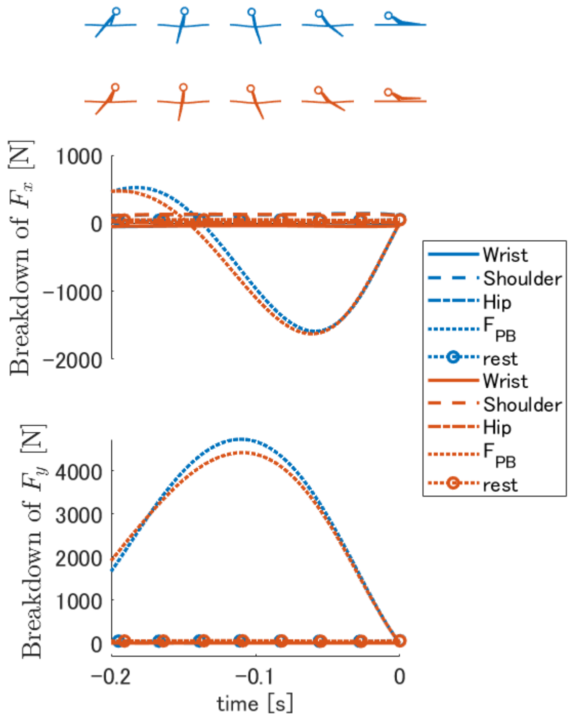

Figure S-4: Breakdown of F_x and F_y into the contributions of the wrist, shoulder, hip joint torques, F_{PB}, and the remaining terms in $[-0.2\,\mathrm{s},\ 0\,\mathrm{s}]$. From the top, the breakdown of F_x and that of F_y are presented. Both $F_x^{F_{PB}}$ and $F_y^{F_{PB}}$ were almost identical to F_x and F_y, respectively.

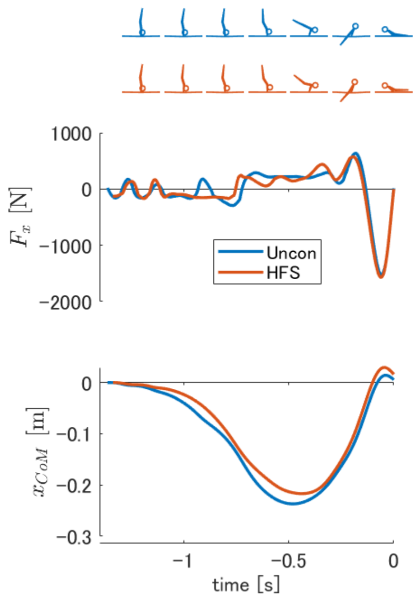

Figure S-5: Horizontal force ($= F_x$) and horizontal position of the CoM ($= x_{CoM}$). From the top, F_x and x_{CoM} are presented. F_x tends to be negative at [start of motion, $-0.8\,\mathrm{s}$], and it tends to be positive at [$-0.7\,\mathrm{s}$, $-0.2\,\mathrm{s}$], which makes x_{CoM} downward convex. This time history utilizes the cumulative effect to decrease x_{CoM}.